Pergamon

Acta mater. 49 (2001) 3719–3726

Acta MATERIALIA

www.elsevier.com/locate/actamat

ROLE OF FLAW STATISTICS IN CONTACT FRACTURE OF BRITTLE COATINGS

P. MIRANDA[1], A. PAJARES[2], F. GUIBERTEAU[1], F. L. CUMBRERA[2] and B. R. LAWN[3]†

[1]Departamento Electrónica e Ingeniería Electromecánica, Escuela de Ingenierías Industriales, Universidad de Extremadura, 06071 Badajoz, Spain, [2]Departamento de Física, Facultad de Ciencias, Universidad de Extremadura, 06071 Badajoz, Spain and [3]Materials Science and Engineering Laboratory, National Institute of Standards and Technology, Gaithersburg, MD 20899, USA

(Received 15 June 2001; accepted 10 July 2001)

Abstract—A flaw statistics analysis is here developed to account for systematic differences between experimentally observed and theoretically predicted critical loads for the initiation of contact-induced radial cracks in brittle coatings on compliant substrates. Specific attention is drawn to deviations in critical load (P_R) data from ideal quadratic dependence on coating thickness (d), i.e. $P_R \propto d^2$, especially at low d values. It is postulated that these deviations are attributable to the existence of distributions in flaw size and location, in relation to the bell-shaped tensile stress fields responsible for initiation of the radial cracks at the coating lower surface. A statistics-based expression is derived for the mean values of P_R in terms of flaw density and size distribution. Data from model bilayers consisting of glass plates of different thicknesses d bonded to polycarbonate substrates are used as an illustrative case study. Controlled pre-abrasion flaws are introduced into the lower glass surfaces before joining into the bilayer configuration, to enable *a priori* characterization of distribution parameters by image analysis. Finite element modelling is used to determine the tensile stress distribution at the coating lower surface. The predicted statistics-based $P_R(d)$ function is shown to fit the data within uncertainty bounds. Implications concerning the continued usefulness of the ideal, $P_R \propto d_2$ relation for designing ceramic coatings for failure resistance are considered.

Keywords: Brittle; Coating; Flaw statistics

1. INTRODUCTION

Brittle coatings afford mechanical, thermal and chemical protection to soft underlayers in many engineering systems (thermal barrier coatings, cutting tools, electronic multilayers, laminated windows) and biomechanical structures (teeth and dental crowns, shells). Such coatings are subject to damage at their top or bottom surfaces from extraneous contact loads. The forms of the damage that occur in the near-contact regions—cone cracks or quasiplastic damage—are well documented [1, 2]. But the most deleterious damage is radial cracking at the bottom surface, from flexure of the coating on the soft support [3–6]. Radial cracks, once initiated, can spread laterally subsurface to the edges of the specimen under any further loading. They are reported to be a primary source of failure in all-ceramic dental crowns [7, 8], and pose a major threat in any system comprising a ceramic outerlayer on a polymeric [5] or metal [9] underlayer.

Analytical relations expressing the critical load P_R for radial cracking in terms of layer thickness d can be derived from the theory of plates on compliant foundations [10], by equating the maximum tensile stress at the bottom of the flexing plate to the bulk strength σ_F of the coating material (as measured in flexure tests with large surface areas). For concentrated contact loading at the top surface, the relation reduces to the simple form $P_R \propto \sigma_F d^2$ (with an additional slow, logarithmic term in Young's modulus ratio) [11, 12]. However, although this relation appears to account for the main trends in $P_R(d)$ data for a wide range of ceramics, systematic deviations have been noted. Forced power-law fits to data for glass coatings with abraded surfaces (to produce controlled flaws) on polycarbonate substrates covering nearly three decades in coating thickness indicated an exponent $m = 1.75$ in $P_R \propto d^m$, i.e. substantially less than 2 [5]. The questions arise: are these deviations significant; and if so, what is their cause?

† To whom all correspondence should be addressed. Fax: +1-301-9268349.

E-mail address: Brian.lawn@nist.gov (B. R. Lawn)

1359-6454/01/$20.00
PII: S1359-6454(01)00280-4

In this study we examine the hypothesis that such deviations in $P_R(d)$ data from ideal quadratic dependence are a consequence of flaw statistics. There is some precedent for this hypothesis from studies of critical loads to initiate cone cracks in Hertzian fracture tests on monolithic glass [13–15], but there the effect is dominated by high downward stress gradients on surface flaws outside the contact area [16]. A consequence of high stress gradients in the latter case is that the critical stresses needed to initiate fracture are size dependent, tending increasingly higher than the bulk strength as the indenting sphere radius diminishes [16–18]. We will show that a somewhat analogous size effect applies to the initiation of radial cracks in bilayer structures, attributable in this case predominantly to the flaw distribution at the coating lower surface. To this end we analyze critical load data from the above-cited study of glass coatings on polycarbonate substrates [5] in terms of a measurable distribution of controlled abrasion flaws. We will argue that the basic $P_R \propto \sigma_F d^2$ relation, even allowing for modification by flaw statistics, remains a sound basis for optimizing layer dimensions and material properties in the design of brittle coatings.

2. STATEMENT OF PROBLEM

Figure 1 is a schematic representation of the contact test arrangement used to produce radial cracks in "model" bilayers consisting of glass coating plates, thickness d and Young's modulus E_c (70.0 GPa), glued with epoxy adhesive to thick, compliant polycarbonate substrates, modulus E_s (2.35 GPa). Contact is made with an indenting tungsten carbide sphere of radius 3.96 mm at load P.† Flaws of characteristic dimension c located in the coating lower surface at radial distance r from the loading axis are subjected to flexural tensile stresses. Radial cracks initiate from most favorably located flaws within this tensile field. Initiation of the radial cracks is monitored *in situ* by observing the contact directly through the bottom of the transparent polycarbonate base layer with a video camera. Experimental critical loads P_R from earlier tests on such glass/polycarbonate bilayers are plotted in Fig. 2 as a function of glass thickness d [5].

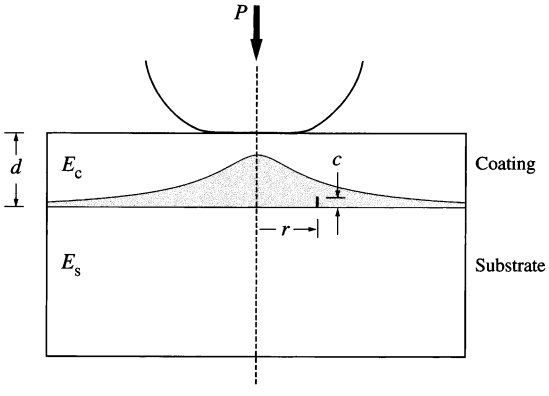

Fig. 1. Schematic of contact at load P on brittle coating of thickness d and modulus E_c bonded to a compliant substrate, modulus E_s. Shaded profile indicates distribution of out-of-plane tensile stresses at lower coating surface. Flaws of characteristic dimension c are located at radial distances r from contact axis.

As indicated (Section 1), an analytical relation for the critical loads can be determined by equating the maximum tensile stress at the coating undersurface to the bulk strength σ_F of the coating material. In the point-contact limit, we obtain [11, 12]

$$P_R = B\sigma_F d^2/\log\,(CE_c/E_s) \qquad (1)$$

where B and C are dimensionless coefficients, i.e. the same above-mentioned form $P_R \propto \sigma_F d^2$ but with an additional slowly-varying logarithmic modulus mismatch term. It is assumed in this relation that σ_F is independent of any characteristic dimension of the bilayer system, notably d. Finite element analysis (FEM) of hypothetical model bilayers (infinitesimally thin well-bonded interfaces, thick substrates, point-contact loading) covering a range of material parameters and coating thicknesses confirms this relation, and enables the coefficient evaluations $B = 1.35$ and $C = 1.00$ [19]. The predicted relation for glass/polycarbonate using these evaluations is included as the line of slope 2 in the logarithmic plot of Fig. 2, using independently measured strength $\sigma_F = 110 \pm 10$ MPa and $E_c/E_s = 70.0$ GPa/2.35 GPa = 29.8 in equation (1) [19]. Deviations of

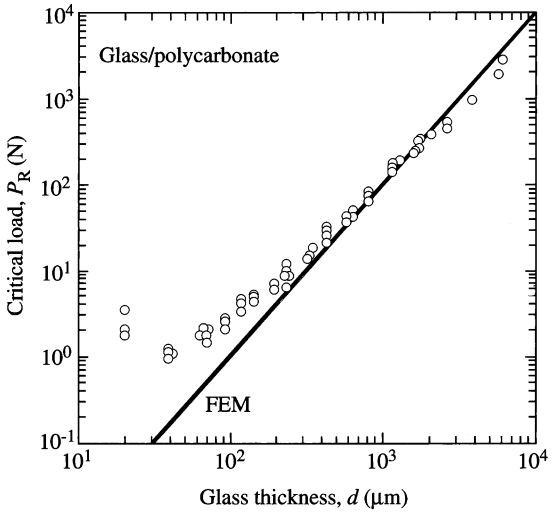

Fig. 2. Critical load P_R to produce radial cracks in glass/polycarbonate bilayer, as function of glass layer thickness d. Data points represent individual contact tests (from [5]). Inclined line is FEM generated prediction, computed for $\sigma_F = 110$ MPa, $E_c/E_s = 29.8$.

† It has been confirmed that P_R is relatively independent of sphere radius in the glass/polycarbonate system, indicating that stresses at the lower surface are not sensitive to the stress distribution at the contact area, i.e. that the loading at the upper surface is effectively one of point contact [19].

the data from the theoretical prediction are apparent, especially at smaller d. Previous analyses effectively ignored such deviations by simply best-fitting the $P_R(d)$ data to equation (1)—such fits for several well-characterized ceramics yield somewhat different coefficients, $B = 2.04$ and $C = 0.94$ [12].

It is implicit in the above assumption of constant σ_F that the critical flaw responsible for radial crack initiation is located at the contact axis where the tensile stress at the coating undersurface is a maximum. In reality, the critical flaw may lie at a radial distance $r>0$, because the flaws are distributed in both size and location. Moreover, the undersurface tensile stresses diminish with radial distance r, over a spatial range that scales with thickness d (geometrical similarity) [19, 20]. Thus, the constant strength assumption is strictly not applicable. According to our hypothesis, the chance of locating a large flaw close to the contact axis within the tensile stress field becomes smaller as d decreases, qualitatively explaining the discrepancies observed in Fig. 2.

3. DISTRIBUTION OF CONTROLLED FLAWS

It is acknowledged that the flaws responsible for fracture in tensile stress fields are distributed in both size and location. It is usually difficult to determine these distributions *a priori* in brittle materials, because the flaws may be submicroscopic and may even lie subsurface. For this reason some researchers use controlled surface abrasion flaws to enable quantitative evaluation by direct microscopy, as well as to reduce (although not eliminate) scatter in critical load data [21]. The glass/polycarbonate experiments represented in Fig. 2 were made on such abraded surfaces, using a slurry of grade 600 SiC grit [5].

Accordingly, an attempt was made to measure the distributions of controlled flaws in glass surfaces under the same abrasion conditions used to obtain the data in Fig. 2. A total of 250 photographs of the abraded surfaces, each covering a selected area ≈ 0.05 mm^2 (with no overlaps between adjacent areas), was taken using Nomarski optical microscopy. An example is shown in Fig. 3. Variations in flaw sizes and separations are evident from simple visual inspection. The photographs were then reduced to binary images by digital analysis. A total of 4.4×10^5 pixelated flaw segments, excluding those segments shorter than 1 μm as noise, was counted over all 250 photographs, corresponding to an average flaw density $\rho\approx3600\ mm^{-2}$ and mean flaw separation ≈17 μm. The largest linear dimension of each counted flaw (from center to center of the endpoint pixels) was then recorded. It is implicit in these measurements that the surface traces provide an appropriate measure of the flaw depth, which would be the case if the flaws are penny-like, as is expected for abrasions with sharp contacts [22]. Figure 4 is a histogram of the number of flaws $N(c)$ counted over 1 μm crack size intervals. The distribution in Fig. 4 has a typically long tail. The data may be considered relatively unreliable at small c, where noise and resolution problems occur; and at large c, because of the relatively small number of cracks in the tail.

In situ indentation tests of the same kind as used to obtain data in Fig. 2 [5] were made to observe the locations of the radial crack starting points within the contact field. A typical example is shown in Fig. 5, for glass thickness $d = 140$ μm. Figure 5(a) is a contact immediately prior to radial crack pop in, Fig. 5(b) immediately after. In this case the radial crack has initiated from a flaw at a distance $r = 45$ μm $= 0.32d$ from the contact center. (There is some indication in Fig. 5(a) that the starting flaw is beginning to open up immediately before pop in.)

4. BASIC STRENGTH AND FLAW STATISTICS RELATIONS

The stress component responsible for initiating radial cracks is the out-of-plane principal "hoop" stress σ at median planes containing the contact axis at the

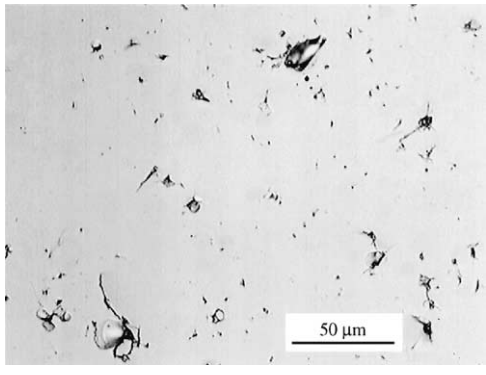

Fig. 3. Micrograph showing distribution of abrasion flaws on glass surface. Surface lightly abraded with slurry of 600 SiC grit, gold-coated and viewed in Nomarski optical illumination.

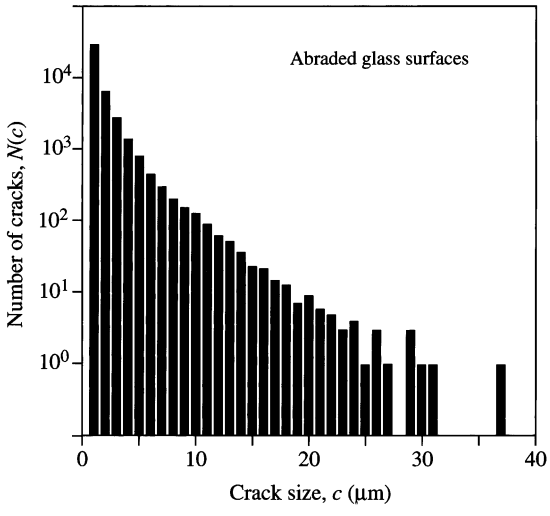

Fig. 4. Flaw size distribution $N(c)$ for abraded glass surfaces, determined from image analysis. Note truncation of data at $c\approx30$ μm.

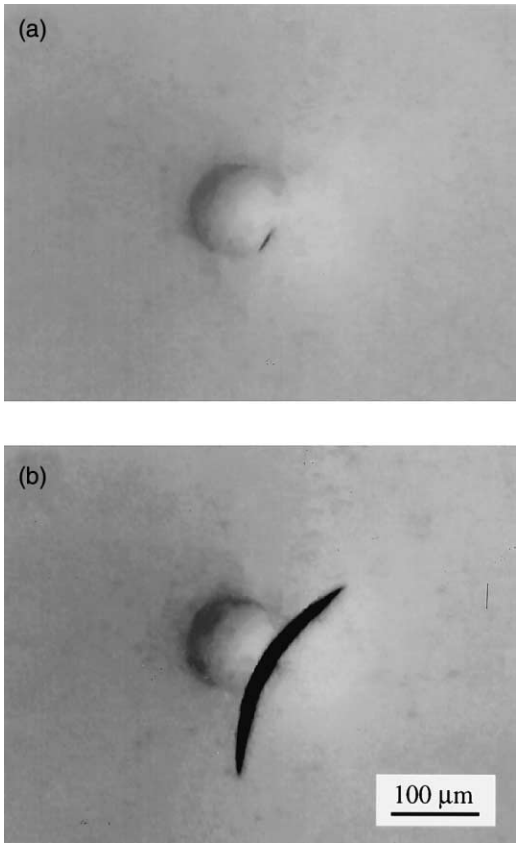

Fig. 5. Successive video frames at load $P = 5.0$ N showing location of radial crack initiation beneath indenter in glass/polycarbonate bilayer, glass thickness $d = 140$ μm. In this case, crack initiates from flaw at radial distance $r = 45$ μm from contact center.

lower coating surface. From an analysis of elastic plates on compliant foundations [10] σ has a maximum value

$$\sigma_m(P,d) = (P/Bd^2)\log(CE_c/E_s) \tag{2}$$

at the contact axis, with B and C defined as above (note equation (2) reduces to equation (1) at $\sigma_m = \sigma_F$). The magnitude of σ falls off monotonically with radial distance r from the contact axis within the lower surface plane according to a relation of the functional form [19]

$$\sigma(P,r,d) = \sigma_m(P,d)f(r/d). \tag{3}$$

As indicated above (Section 2), this relation reflects geometrical similarity in the stress field, in which the relative stress σ/σ_m at any given relative location r/d is uniquely determined for any given material bilayer system. Figure 6 plots the (FEM-generated) $f(r/d)$ function for glass/polycarbonate bilayers ($E_c/E_s = 29.8$) [19]. Note the substantial falloff with radial distance, from $f = 1$ at $r/d = 0$ to $f < 0.5$ at

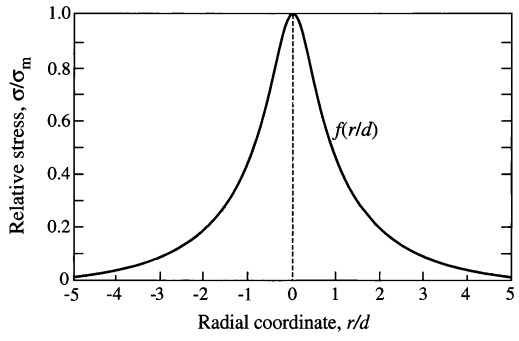

Fig. 6. FEM-generated function $f(r/d)$ in equation (3) (from [19]), calculated using $E_c/E_s = 29.8$ for glass/polycarbonate bilayer.

$r/d = 1$. On the other hand, stress gradients along flaw coordinates normal to the lower surface tend to be negligibly small comparatively, at least in the domain $c \ll d$ (unlike in the case of cone cracks where downward gradients dominate the stress field characteristics).

Consider a given flaw at radial distance r in the lower surface of the coating in Fig. 1. For this flaw to initiate a radial crack at contact load P, it would have to satisfy the Griffith relation

$$c = [T/\psi\sigma(P,r,d)]^2 \equiv c_*(P,r,d) \tag{4}$$

with $\sigma(r,P,d)$ determined from equation (3), T the coating toughness (here assumed single-valued = K_{IC}, i.e. no R-curve), and ψ a crack geometry coefficient. In any given contact event, the inhomogeneous contact tensile stress field will search for the "weakest link" in the population, so that the critical flaw will be the one that satisfies equation (4) at the lowest value of P. Again, we point out that the contact field will have increasing difficulty in locating a particularly large flaw when the coating thickness d approaches the mean separation distance between neighbors.

At this point it is necessary to introduce statistical elements into the description. Consider a flaw population of density ρ and size distribution $N(c)$ as defined above. Define a probability $\Gamma(P,d)\mathrm{d}P$ for the Griffith condition to be satisfied between P and $P + \mathrm{d}P$ within a given indentation field. For actual radial crack initiation within this load interval it is necessary that the specimen should survive up to load P. Then the probability $\Phi(P,d)\mathrm{d}P$ that a radial crack initiates between P and $P + \mathrm{d}P$, and not before, may be written as the product

$$\Phi(P,d)\,\mathrm{d}P = \Omega(P,d)\Gamma(P,d)\,\mathrm{d}P \tag{5}$$

where the function $\Omega(P,d)$ defines the probability of survival to load P. The two functions on the right side of equation (5) are interrelated (Appendix A)

$$\Omega(P,d) = \exp[-\int_0^P \Gamma(P',d)\,dP']. \quad (6)$$

The $\Gamma(P,d)$ term may be determined by integrating over the lower surface area of the coating:

$$\Gamma(P,d) = \int_0^\infty 2\pi r\rho S[c_*(P,r,d)]\,dr \quad (7)$$

where ρ is the flaw density, here assumed uniform, and $S(c)$ is the probability density for any given flaw to have a size c, defined by

$$S(c) = N(c)/\int_0^\infty N(c')\,dc'. \quad (8)$$

Now we may compute the mean critical contact load P_R to initiate a radial crack in a coating of thickness d

$$P_R(d) = \langle P\rangle = \int_0^\infty P\Phi(P,d)\,dP. \quad (9)$$

Substituting equations (5)–(7) into equation (9) yields

$$P_R(d) = \int_0^\infty \{\int_0^\infty 2\pi r\rho S[c_*(P,r,d)]\,dr\} \quad (10)$$
$$\exp\{-\int_0^P\int_0^\infty 2\pi r\rho S[c_*(P',r,d)]\,dr\,dP'\}P\,dP.$$

5. DATA ANALYSIS

Equation (10) may now be integrated numerically to determine the function $P_R(d)$. We do this here for the glass/polycarbonate bilayer system using the following quantities: experimentally averaged flaw density ρ and $N(c)$ from Section 3 (to evaluate $S(c)$ in equation (8)) for our abraded glass surfaces; FEM-computed $f(r/d)$ for $E_c/E_s = 29.8$ for glass/polycarbonate from Fig. 6 (in conjunction with equations (2) and (3)), along with $\psi = 2/\pi^{1/2}$ (penny cracks) and toughness $T = 0.67$ MPa.m$^{1/2}$ for glass [19], to evaluate $c_*(P,r,d)$ in equation (4). Figure 7 plots the computed $P_R(d)$ function (solid curve), along with computational uncertainty bounds (evaluated from standard deviations $[\langle P^2\rangle - \langle P\rangle^2]^{1/2}$) (dashed curves). The bounding curves overlap the experimental standard deviation error bars (evaluated here by grouping the data in Fig. 2 within coating thickness increments) over the bulk of the range of d, except at the extremes of the range where the predictions (and also the experimental data) are less reliable [5].

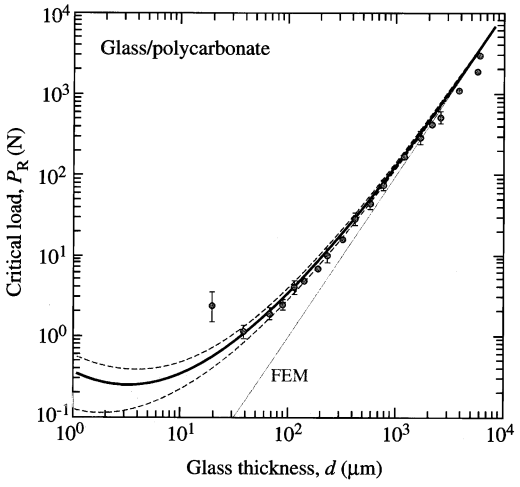

Fig. 7. Statistically-based $P_R(d)$ function from [10], plotted as solid curve with dashed standard deviation envelopes, for glass plates with abraded undersurfaces bonded to polycarbonate substrates. Data with error bars are means and standard deviations obtained by grouping data in Fig. 2 over d increments (data without error bars are single test values). Inclined line is FEM generated prediction from Fig. 2.

As may be expected, the computed $P_R(d)$ curve tends asymptotically to the limiting $P_R \propto d^2$ line at large d, corresponding to a single-valued bulk strength of $\sigma_F = 110$ MPa (Section 2). This limiting strength in turn corresponds to a limiting flaw size $c_* \approx 30$ μm in equation (4). Observe that the $N(c)$ distribution in Fig. 4 truncates around this value. At the opposite end of the thickness spectrum, at $d \approx 4$ μm, the $P_R(d)$ curve has a minimum. This simply means that at very small d the *decrease* in P_R associated with increased lower-surface stresses is ultimately dominated by an *increase* in P_R associated with the increased difficulty in locating a large flaw. Note that at the lower limit of data in Fig. 7 ($d = 20$ μm) the contact stress field gradients over the through-thickness dimension of the largest flaws will be high (analogous to the high gradients experienced in the cone crack problem [16]), perhaps accounting for the apparent deviation between the last data point and calculated curve in this region.

6. DISCUSSION

We have used a flaw statistical treatment to account for deviations from the ideal $P_R \propto d^2$ functional dependence in the contact loading of brittle coatings on compliant substrates, taking data from a model glass/polycarbonate bilayer system as an illustrative case study. Evaluation of the statistically averaged

$P_R(d)$ function in equation (10) requires predetermination of just two key functions: $N(c)$ (from image analysis), to evaluate $S(c)$ in equation (8); and $\sigma(P,r,d)$ in equation (3), from computation of $f(r/d)$ (using FEM) in conjunction with $\sigma_m(P,d)$ in equation (2), along with input ψ and T values, to determine $c_*(P,r,d)$ in equation (4). This approach does require exacting numerical analysis (to avoid convergence problems), but has no adjustable parameters. The "agreement" between computed $P_R(d)$ function and corresponding experimental data in Fig. 7, especially in the central regions of the plot, supports our hypothesis that flaw statistics is responsible for the observed deviations.

At the same time, it is acknowledged that any such agreement between theory and experiment in Fig. 7 can not be considered as strong validation of the input parameters. Our analysis is not without its sources of uncertainty. Predeterminations of abrasion flaw density ρ and size distribution $N(c)$ from image analysis are subject to experimental error. The parameter $\psi = 2/\pi^{1/2}$ used in equation (4) assumes flaws of ideal penny-like crack geometry (appropriate to point-contact abrasion) [22], devoid of any residual stresses from the abrasion contact process [23]. No account has been taken of flaw orientation (although this is less likely to be an important source of error, since the tensile field acting on the flaws is largely biaxial). Likewise, the representative glass toughness $T = 0.67$ MPa.m$^{1/2}$ used in equation (4) is sensitive to extraneous factors such as loading rate and environment [24, 25]. Variations in any of these parameters will inevitably cause shifts in the computed $P_R(d)$ curve in Fig. 7.

Notwithstanding these qualifications, equation (1) is a valuable relation for elucidating the role of layer thickness and material variables on critical loads for radial cracking in brittle coatings [11]. In preceding studies the approach has simply been to force-fit equation (1) to experimental $P_R(d)$ data over the coating thickness range (typically 100 μm$<d<$10 mm) [12, 26], thus providing accurate representation only in the mid-range regions. The corresponding FEM-generated $P_R(d)$ function, while affording a meaningful asymptotic limit to the statistics-based function equation (10) at large d, underestimates the $P_R(d)$ data over the bulk of the thickness range (by more than an order of magnitude at small d end of the data range in Fig. 7). Hence equation (1), with due allowance for inaccuracies in extreme regions of the thickness range, may be retained as a basis for designing damage-resistant coatings, with the FEM-generated function providing a conservative lower bound.

Data on other brittle coating systems, e.g. polycrystalline ceramics [12], show similar $P_R(d)$ data trends to those in Fig. 2, i.e. an apparent exponent m in $P_R \propto d^m$ less than 2. In principle, the statistical analysis presented here should apply to these other coating systems equally well. However, in our case study we have used controlled (abrasion) flaws on glass surfaces, where the surface flaw distributions can be measured *a priori* by microscopic observation and image analysis. Analogous *a priori* measurements of flaw distributions are not always practical in polycrystalline ceramics, especially in fine grain microstructures, where critical flaws may be submicroscopic (and may even lie subsurface). In the absence of any such prior knowledge of the flaw distributions, we are limited to the above-mentioned averaged (experimentally calibrated) or conservative, lower-bound (FEM) predictions of the $P_R(d)$ function.

The asymptotic limit of the statistics-based $P_R(d)$ function at large d corresponds to a contact field with the largest flaw in the population at the lower coating surface ideally located exactly at the contact axis. In reality, the largest flaws will lie at some radial distance from the contact axis, so cracking will tend to occur at a smaller, closer flaw. Since the spatial range of the tensile stress field scales with d (geometrical similarity), the "effective strength" $\sigma = \sigma_{eff}$ determined from the Griffith relation in equation (4) will tend to increase monotonically with decreasing d. Figure 8 plots σ_{eff} as a function of d for the glass coatings, determined by inserting calculated values of $P = P_R$ from equation (10) (together with standard deviation error bounds) into equation (2), using B and C values from the FEM calibration. The bulk strength σ_F (as measured in flexure tests with large surface areas) is then given by the asymptotic approximation at large d. At small d, the curve extrapolates rapidly to unrealistically high values, exceeding the theoretical strength of glass ($\approx$10 GPa) at $d<10$ μm. However, the curve in Fig. 8 has been extrapolated well beyond the lower limit of the experimental data ($d = 20$ μm, Fig. 7) where the stress gradients are large and the calculations are more uncertain. The

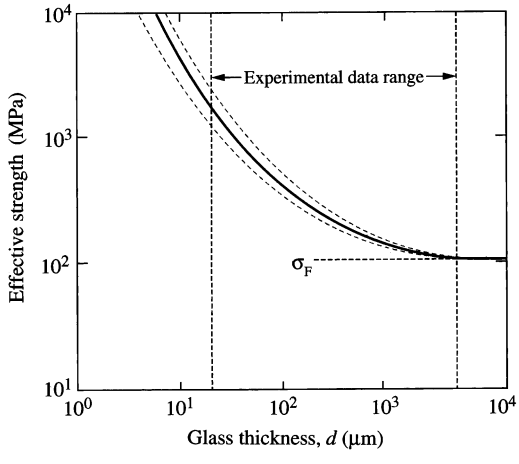

Fig. 8. Effective strength σ_{eff} of abraded glass layer on polycarbonate substrate, as function of thickness d. Curve plus standard deviation bounds computed from equation (2) at $P = P_R(d)$, using $P_R(d)$ calculated from equation (10). Experimental data range in Fig. 7 indicated. At large d, σ_{eff} tends asymptotically to the bulk strength σ_F of abraded glass.

dangers of extrapolating fracture predictions beyond the data ranges have been well documented in the literature [27, 28].

The plot in Fig. 8 nevertheless has implications for thin films ($d<1$ μm, say) subjected to concentrated loads. It suggests that the effective strengths of thin films may be considerably higher than for thick coatings, at least where the flaw distributions do not differ substantially from those in the bulk material. (However, similar strength enhancement may not be realized in more uniform tensile fields, e.g. from residual thermal expansion mismatch stresses.)

The main goal of this study has been to demonstrate the importance of flaw statistics in any complete account of critical load data trends for brittle coatings on soft substrates in contact loading. A secondary issue that arises is the possible deconvolution of some characteristic flaw distribution function, in our case the quantity $\rho S(c)$ in equation (10), from the raw $P_R(d)$ data. One could then attempt to relate this flaw distribution function to some pertinent microstructural variable (e.g. grain size) for a given ceramic coating. The argument might be made that this composite $\rho S(c)$ function could be more directly obtained from conventional biaxial strength testing of specimens of different surface test areas. However, this would require an extensive number of specimens, with one data point per specimen, and exacting test fixtures. Contact testing, with simpler testing protocol and the capacity for multiple tests per specimen, would appear to afford a much simpler and more economical experimental route.

Finally, mention may be made of the generality of the methodology proposed here. Given a suitable stress analysis, analytical or numerical (e.g. FEM), there is nothing to preclude extension of the analysis to trilayers [20] or multilayers, or even to more complex composite geometries.

Acknowledgements—Support for this work was provided by the Junta de Extremadura-Consejeria de Educación, Ciencia y Tecnología y el Fondo Social Europeo, Spain (Grant IPR00A084), by internal NIST funds and by an NIDR grant (PO1 DE10976).

REFERENCES

1. Lawn, B. R., Padture, N. P., Cai, H. and Guiberteau, F., *Science*, 1994, **263**, 1114.
2. Lawn, B. R., *J. Am. Ceram. Soc.*, 1998, **81**, 1977.
3. An, L., Chan, H. M., Padture, N. P. and Lawn, B. R., *J. Mater. Res.*, 1996, **11**, 204.
4. Lee, K. S., Wuttiphan, S., Hu, X. Z., Lee, S. K. and Lawn, B. R., *J. Am. Ceram. Soc.*, 1998, **81**, 571.
5. Chai, H., Lawn, B. R. and Wuttiphan, S., *J. Mater. Res.*, 1999, **14**, 3805.
6. Jung, Y. G., Wuttiphan, S., Peterson, I. M. and Lawn, B. R., *J. Dent. Res.*, 1999, **78**, 887.
7. Kelly, J. R., *Ann. Rev. Mater. Sci.*, 1997, **27**, 443.
8. Kelly, J. R., *J. Prosthet. Dent.*, 1999, **81**, 652.
9. Zhao, H., Hu, X. Z., Bush, M. B. and Lawn, B. R., *J. Mater. Res.*, 2000, **15**, 676.
10. Timoshenko, S. and Woinowsky-Krieger, S., *Theory of Plates and Shells*, 2nd ed. McGraw-Hill, New York, 1959, Chap. 8.
11. Lawn, B. R., Lee, K. S., Chai, H., Pajares, A., Kim, D. K., Wuttiphan, S., Peterson, I. M. and Hu, X., *Adv. Eng. Mater.*, 2000, **2**, 745.
12. Rhee, Y. -W., Kim, H. -W., Deng, Y. and Lawn, B. R., *J. Am. Ceram. Soc.*, 2001, **18**, 1066.
13. Argon, A. S., *Proc. R. Soc. Lond.*, 1959, **A250**, 482.
14. Oh, H. L. and Finnie, I., *J. Mech. Phys. Solids*, 1967, **15**, 401.
15. Poloniecki, J. D. and Wilshaw, T. R., *Nature*, 1971, **229**, 226.
16. Frank, F. C. and Lawn, B. R., *Proc. R. Soc. Lond.*, 1967, **A299**, 291.
17. Lawn, B. R. and Wilshaw, T. R., *J. Mater. Sci.*, 1975, **10**, 1049.
18. Lee, S. K., Wuttiphan, S. and Lawn, B. R., *J. Am. Ceram. Soc.*, 1997, **80**, 2367.
19. Kim, H.-W., Deng, Y., Miranda, P., Pajares, A., Kim, D. K., Kim, H.-E. and Lawn, B. R., *J. Am. Ceram. Soc.* (in press).
20. Miranda, P., Pajares, A., Guiberteau, F., Cumbrera, F. L. and Lawn, B. R., *J. Mater. Res.*, 2001, **16**, 115.
21. Langitan, F. B. and Lawn, B. R., *J. Appl. Phys.*, 1969, **40**, 4009.
22. Wiederhorn, S. M. and Lawn, B. R., *J. Am. Ceram. Soc.*, 1979, **62**, 66.
23. Marshall, D. B. and Lawn, B. R., *J. Am. Ceram. Soc.*, 1961, **64**, C6.
24. Wiederhorn, S. M., *J. Am. Ceram. Soc.*, 1969, **52**, 99.
25. Wiederhorn, S. M. and Bolz, L. H., *J. Am. Ceram. Soc.*, 1970, **53**, 543.
26. Lee, K. S., Rhee, Y. -W., Blackburn, D. H., Lawn, B. R. and Chai, H., *J. Mater. Res.*, 2000, **15**, 1653.
27. Wiederhorn, S. M., Fuller, E. R., Mandel, J. and Evans, A. G., *J. Am. Ceram. Soc.*, 1976, **59**, 403.
28. Wiederhorn, S. M., in *Fracture 1977, Fourth International Conference on Fracture*, ed. D. M. R. Taplin. Vol. 3. University of Waterloo Press, Waterloo, Canada, 1977, p. 893.

APPENDIX A

A.1. Evaluation of $\Omega(P,d)$

Let $\Omega(P + dP,d)$ be the probability of survival up to load $P + dP$. This can be written

$$\Omega(P + dP,d) = \Omega(P,d)\Omega(dP,d)$$

where $\Omega(dP,d)$ is the probability of surviving between P and $P + dP$. Then

$$\Omega(dP,d) = 1-\Gamma(P,d)\, dP$$

where $\Gamma(P,d)$ is the probability density defined in equation (7) of the text. Thus

$$\Omega(P + dP,d) = \Omega(P,d)[1-\Gamma(P,d)\, dP].$$

Comparing this last equation with the Taylor expansion

$$\Omega(P + dP,d) = \Omega(P,d) + [d\Omega(P,d)/dP]\, dP + \ldots$$

we have

$$d\Omega(P,d)/\Omega(P,d) = -\Gamma(P,d)\, dP.$$

Integration yields

$$\Omega(P,d) = \exp\left[-\int_0^P \Gamma(P',d)\, dP'\right]$$

which is equation (6) in the text.